Interactions of Earth Atmospheric Oxygen and Fuel Moisture in Smouldering Wildfires

Xinyan Huang, Guillermo Rein*

Department of Mechanical Engineering, Imperial College London, United Kingdom

Abstract

Vegetation, wildfire and atmospheric oxygen on Earth have changed throughout geological times, and are dependent on each other, determining the evolution of ecosystems, the carbon cycle, and the climate, as found in the fossil record. Previous work in the literature has only studied flaming wildfires, but smouldering is the most persistent type of fire phenomena, consuming large amounts of biomass. In this study, the dependence of smouldering fires in peatlands, the largest wildfires on Earth, with atmospheric oxygen is investigated. A physics-based computational model of reactive porous media is developed which was previously validated against experiments. Simulations are conducted for wide ranges of atmospheric oxygen concentrations and fuel moisture contents to find thresholds for ignition and extinction. Results show that the predicted rate of spread increases in oxygen-rich atmospheres, while it decreases over wetter fuels. A novel nonlinear relationship between critical oxygen and critical moisture is found. More importantly, we show that compared to previous work on flaming fires, smouldering fires can be ignited and sustained at a substantially higher moisture content ($> 100\%$), and at a substantially lower oxygen concentration ($\sim 12\%$). This defines a possible lower oxygen threshold for wildfire and could help interpret the char remains and paleo fire activities seen in the fossil record.

Keywords: Fire, Vegetation, Paleo fire, Modelling, Peat, Soil, Ignition

1. Introduction

Vegetation, wildfire and atmospheric oxygen on Earth have changed throughout geological times (Lovelock, 1979; Lenton and Watson, 2000), and are dependent on each other, determining the evolution of ecosystems, the carbon cycle, and the climate, as found in the fossil record (Belcher and McElwain, 2008; Belcher et al., 2010; Lenton, 2013). Increasing the oxygen concentration (X_{O_2}, percentage by volume) above the present-day level of 21%, the ignition probability of vegetation on land increases (Lovelock and Lodge, 1972; Lenton and Watson, 2000). The influence of atmospheric oxygen on the flammability of Earth ecosystems has been investigated in Wildman et al. (2004); Belcher and McElwain (2008); Belcher et al. (2010); Watson and Lovelock (2013). Most of these studies considered flaming wildfires, and their results suggested that below a critical oxygen concentration ($X^*_{O_2}$) between

*. Corresponding author. Tel: +44 (0)20 7594 7036.
Email address: g.rein@imperial.ac.uk (Guillermo Rein)

12 to 16%, fire activity is not possible. But compared to flaming, smouldering combustion is the most persistent type of fire phenomena on Earth, consuming large amounts of biomass and burning for very long periods of time (years or centuries) (Rein, 2013). However, the interdependence of atmospheric oxygen and fuel moisture on smouldering wildfire has not yet been studied until now.

Smouldering combustion is the slow, low-temperature, flameless burning of porous fuels and the most persistent type of combustion, different from flaming combustion (Ohlemiller, 1985; Rein, 2013). Smouldering is the dominant phenomena in wildfires in natural deposits of peat which are the largest fires on Earth. Compared to flaming fires, smouldering fires can be initiated by weaker ignition sources, and are more difficult to suppress (Rein, 2013). Therefore, understanding the dependence of smouldering wildfires with atmospheric oxygen is crucial to estimate the fire threshold on Earth's vegetation throughout geological times. In the literature (Watson and Lovelock, 2013; Wildman et al., 2004; Belcher and McElwain, 2008), two critical oxygen values have been studied for flaming fires: (1) critical oxygen for ignition, below which fire cannot be initiated by any ignition source, and (2) critical oxygen for fire spread (or extinction), below which an existing fire cannot be sustained or extinction occurs.

For wildfires, similar critical values have been found associated to fuel moisture (Frandsen, 1997; Rein et al., 2008; Benscoter et al., 2011; Watson and Lovelock, 2013; Watts, 2013). Atmospheric oxygen and fuel moisture are two of the most crucial factors governing the ignition and spread of wildfires throughout Earth's history, more important than other properties like mineral content, chemical composition, and bulk density. Organic soils like peat are porous and are able to hold a wider range of moisture contents [1] (MC), ranging from about 10% under drought conditions to well in excess of 300% under flooded conditions (Benscoter et al., 2011; Rein, 2013). Similar to flaming fires, the fuel moisture represents a significant energy sink to prevent smouldering fires.

Watson and Lovelock (2013) studied experimentally the probability of flaming ignition and the rate of flame spread of cellulosic paper with varying MC and X_{O_2}. For their experiments of flaming ignition, the paper tape was enclosed inside a bell jar and subject to the application of an energetic electric discharge (7.5 kV and 0.12 A). The duration of discharge for ignition was measured for various combination of oxygen concentration and MC. For their experiments of flame spread and extinction, thin shredded paper ∼2.5 mm wide and with MC from 0 to 150% was laid out in a stainless-steel wire mesh (5 cm wide, 2 cm deep, and 12 cm long), and placed inside a bell jar, flushed by air enriched in O_2 or N_2. The ignition was attempted by a pilot methane burner (regular ignition source) or by the burning dry paper (strong ignition source). The $X^*_{O_2}$ and MC* to suppress flame spread and the spread rate were found (Watson and Lovelock, 2013). Based on these experiments, they proposed a linear correlation, $\mathrm{MC}^* = 8X^*_{O_2} - 128$, describing Earth's wildfire threshold as a function of X_{O_2}.

Several studies have investigated the critical MC under the current atmosphere ($X_{O_2} \sim 21\%$) for smouldering peat fires through both experimental (Frandsen, 1997; Rein et al., 2008; Benscoter et al., 2011) and computational (Huang et al., 2015; Huang and Rein,

1. Moisture content (MC) is defined in dry basis as the mass of water divided by the mass of a dry sample, expressed as %.

2015) approaches. Their results confirmed for a given X_{O_2}, MC dominates smouldering, and different critical values exist for ignition (MC^*_{ig}) and extinction (MC^*_{ex}). A limited number of studies looked into the influence of oxygen on smouldering fuels for a given MC. Belcher et al. (2010) found that the smouldering could not be sustained below a critical X_{O_2} of 16% for a dry moss peat under a quiescent flow condition. Hadden et al. (2013) found that oven-dried moss peat (MC $\leq$10%) aided by a weak wind could be ignited under a X_{O_2} as low as 11%. So far, there is no study, especially no computational study, available in the literature investigating the interaction of atmospheric oxygen and fuel moisture on smouldering wildfires.

In this work, a computational model of smouldering combustion is used to simulate peat fires under varying oxygen concentration and moisture content. The X_{O_2} and MC for smouldering are found, which will help interpret the char remains and paleo fire activity seen in the fossil record.

2. Computational model

2.1. Modelling setup

In order to extend the study of $X^*_{O_2}$ to smouldering wildfires, both the smouldering ignition and fire spread are modelled in a one-dimensional (1D) model, as shown in Fig. 1. For ignition, a 3-cm thick peat sample is simulated, similar to the bench-scale experiment in Hadden et al. (2013). This small sample is heated by constant and strong external irradiation (30 kW/m^2), and the heating duration is varied to find the critical value for successful ignition under varying $X^*_{O_2}$ and MC. For fire spread, a 12-cm thick peat sample including 1-cm dry peat on the top and 11-cm wet peat on the bottom is simulated. The dry fuel is used to guarantee a successful ignition, in agreement with the flaming spread experiment of Watson and Lovelock (2013) and Frandsen (1997).

The influence of MC on smouldering peat has been studied computationally at X_{O_2} = 21% perviously in Huang et al. (2015) and Huang and Rein (2015). The influence of varying X_{O_2} on smouldering peat fires has been studied computationally with dry peat (10% MC)

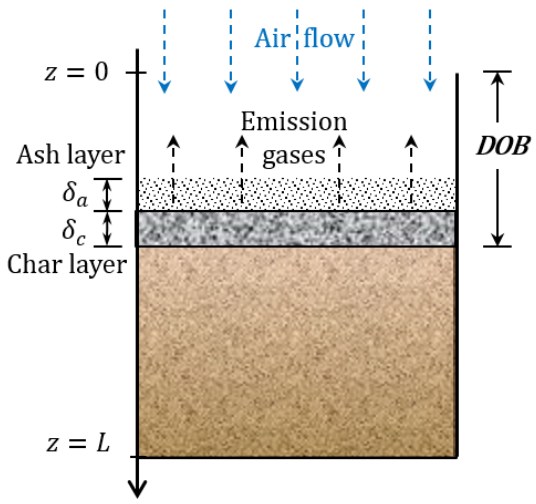

Figure 1: Sketch of the computational domain for the burning peat during smouldering spread with the associated depth of burn (DOB) .

in Huang and Rein (2016). This 1D model, developed in the open-source code Gpyro, is also used for this study. The details of Gpyro can be found in Lautenberger and Fernandez-Pello (2009). The smouldering model solves transient equations for Eq. (1) condensed-phase mass conservation, Eq. (5) condensed-phase species conservation (assuming thermal equilibrium with the gas phase), Eq. (3) condensed-phase energy conservation, Eq. (4) gas-phase mass conservation, Eq. (5) gas-phase species conservation and Eq. (6) gas-phase momentum conservation (Darcy's law):

$$\frac{\partial \overline{\rho}}{\partial t} = -\dot{\omega}_{fg}^{'''} \tag{1}$$

$$\frac{\partial \left(\overline{\rho} Y_i\right)}{\partial t} = \dot{\omega}_{fi}^{'''} - \dot{\omega}_{di}^{'''} \tag{2}$$

$$\frac{\partial (\overline{\rho}\overline{h})}{\partial t} + \frac{\partial \left(\dot{m}^{''} h_g\right)}{\partial z} = \frac{\partial}{\partial z}\left(\overline{k}\frac{\partial T}{\partial z}\right) + \sum_{k=1}^{K}\left(-\dot{\omega}_{di,k}^{'''}\right)\Delta H_k \tag{3}$$

$$\frac{\partial \left(\rho_g \overline{\psi}\right)}{\partial t} + \frac{\partial \dot{m}^{''}}{\partial z} = \dot{\omega}_{fg}^{'''} \tag{4}$$

$$\frac{\partial \left(\rho_g \overline{\psi} Y_i\right)}{\partial t} + \frac{\partial (\dot{m}^{''} Y_j)}{\partial z} = -\frac{\partial}{\partial z}\left(\overline{\psi}\rho_g D\frac{\partial Y_j}{\partial z}\right) + \dot{\omega}_{fj}^{'''} - \dot{\omega}_{dj}^{'''} \tag{5}$$

$$\dot{m}^{''} = -\frac{\overline{K}}{\nu}\frac{\partial P}{\partial z} \qquad (P = \rho_g R_s T) \tag{6}$$

Each condensed-phase species is assumed to have constant and temperature-independent properties (e.g. bulk density, specific heat, and porosity). All gaseous species have unit Schmidt number, and the same diffusion coefficient and specific heat. The averaged properties in each cell are calculated by weighting the mass fraction or the volume fraction.

At the free surface ($z = 0$), a convection coefficient $h_{c,0} = 10$ W/m^2-K capturing the effect of wind, and the surface reradiation ($\varepsilon = 0.95$) are modelled for boundary conditions. The heat-mass transfer analogy is used, $h_{m,0} \approx 20$ g/m^2-s for gas species conservation. The ambient pressure and temperature are constant at 1 atm and 300 K. An external irradiation ($\dot{q}_e^{''}$) is applied as an ignition source, which is used to capture all ignition sources (e.g. lightening, flaming, volcano eruption and self-ignition) in a general manner. At the bottom boundary ($z = L$), a small heat loss is modelled with $h_{c,L} = 3$ W/m^2-K; and there is no mass flux $\dot{m}^{''} = 0$ kg/m^2-s (same as Huang et al. (2015)).

Gpyro adopts a fully implicit formulation is adopted for the solution of all equations (Lautenberger and Fernandez-Pello, 2009). The sample height during spread is equal to the sum of the heights of each cell, $H_t = \sum_{n=1}^{N} \Delta z_n$, which depends on mass conservation and density. Simulations were run with an initial cell size of $\Delta z = 0.1$ mm, and initial time step of 0.02 s. Reducing the cell size and time step by a factor of 2 gives little difference in results, so this discretisation is acceptable.

2.2. Chemical kinetics

A general heterogeneous reaction, k, in the mass basis is written as

$$A_k + \sum_{j=1}^{N} \nu_{j,k}^{'} \text{gas } j \rightarrow \nu_{B,k} B_k + \sum_{j=1}^{N} \nu_{j,k}^{''} \text{gas } j. \tag{7}$$

For a small particle of uniform temperature T, the non-dimensional conversion rate ($\dot{\omega}_k^*$) from species A to B can be expressed by Arrhenius law as

$$\dot{\omega}_k^* = Z_k e^{-E_k/RT} f\left(m_A^*\right) g\left(Y_{O_2}\right), \tag{8}$$

where Z_k and E_k are the pre-exponential factor and the activation energy, respectively.

Here, $f(m_A^*)$ and $g(Y_{O_2})$ are the reaction model for the reactant A and O_2:

$$f\left(m_A^*\right) = \left(m_A^*\right)^{n_k} = \left(\frac{m_A}{m_{sA,0}}\right)^{n_k} \tag{9}$$

$$g(Y_{O_2}) = \begin{cases} 1 & \text{(inert atmosphere)} \\ (1+Y_{O_2})^{n_{O_2,k}} - 1 & \text{(oxidative atmosphere)} \end{cases} \tag{10}$$

where n_k and $n_{O_2,k}$ are the order of reaction and oxygen, respectively.

Both $\dot{\omega}_k^*$ and m_A^* are normalized to a characteristic mass of the particle, $m_A^* = m_A/m_{sA,0}$, where the subscript "$sA,0$" represents the initial mass of source species for A, discussed more in Huang and Rein (2016). Therefore, the destruction rate of A, formation rate of B, and corresponding heat of reaction in the reaction k are $\dot{\omega}_{dA_k} = \dot{\omega}_k^* m_{sA,0}$, $\dot{\omega}_{fB_k} = \dot{\omega}_k^* \nu_{B,k} m_{sA,0}$, and $\dot{Q}_k = \dot{\omega}_{dA_k} \Delta H_k$, respectively, where subscripts "d" and "f" represent the destruction and the formation, and ΔH_k is the heat of reaction.

Huang and Rein (2014, 2016) investigated decomposition schemes of different complexities using thermogravity data for six different peat types from Scotland, Siberia, Ireland, and China. The best kinetics scheme was found to be 5-step: (1) Drying (dr), (2) Peat pyrolysis (pp), (3) Peat oxidation (po), (4) β-Char oxidation (βo), and (5) α-Char oxidation (αo) as

$$\begin{cases} \text{Peat} \cdot \nu_{w,dr}\text{H}_2\text{O} \rightarrow \text{Peat} + \nu_{w,dr}\text{H}_2\text{O(g)} & (dr) \\ \text{Peat} \rightarrow \nu_{\alpha,pp}\alpha\text{-Char} + \nu_{g,pp}\text{Gas} & (pp) \\ \text{Peat} + \nu_{O_2,po}\text{O}_2 \rightarrow \nu_{\beta,po}\beta\text{-Char} + \nu_{g,po}\text{Gas} & (po) \\ \beta\text{-Char} + \nu_{O_2,\beta o}\text{O}_2 \rightarrow \nu_{a,\beta o}\text{Ash} + \nu_{g,\beta o}\text{Gas} & (\beta o) \\ \alpha\text{-Char} + \nu_{O_2,\alpha o}\text{O}_2 \rightarrow \nu_{a,\alpha o}\text{Ash} + \nu_{g,\alpha o}\text{Gas} & (\alpha o) \end{cases} \tag{11}$$

where subscripts w, p, α, β, and a represent five condensed species: water, peat, α-char, β-char, and ash (see Tables and), in addition to four gaseous species: oxygen, nitrogen, water vapour, and emission gases.

2.3. Parameter selection

The solid ($\psi_i = 0$) thermo-physical properties, $\rho_{s,i}$, $k_{s,i}$, c_i of peat, char, and ash are selected from Jacobsen et al. (2003). The porosity is calculated from the bulk and solid densities (ρ_i and $\rho_{s,i}$) as

$$\psi_i = 1 - \frac{\rho_i}{\rho_{s,i}} \tag{12}$$

where the bulk densities of all species for this moss peat were measured in Hadden et al. (2013), all listed in Table 1.

Table 1: Physical parameters of condensed-phase species where $\rho_{s,i}$, $k_{s,i}$, and c_i are from Jacobsen et al. (2003), and $\rho_{i,0}$ is from Hadden et al. (2013).

Species (i)	$\rho_{s,i}$ (kg/m^3)	$\rho_{i,0}$ (kg/m^3)	$\psi_{i,0}$ (-)	$k_{s,i}$ (W/m-K)	c_i (J/kg-K)
water	1000	1000	0	0.6	4186
peat	1500	200 [a]	0.867	1.0	1840
α-char	1300	185	0.962	0.26	1260
β-char	1300	185	0.962	0.26	1260
ash	2500	35	0.997	1.2	1380

a. Bulk density of oven-dried peat (MC = 10%) is 200(1+MC) = 220 kg/m^3.

The effective thermal conductivity includes the radiation heat transfer across pores [2] as

$$k_i = k_{s,i}(1 - \psi_i) + \gamma_i \sigma T^3 \tag{13}$$

where $\gamma_i = 10^{-4} \sim 10^{-3}$ m, dependent on pore size as $\gamma_i \approx 3d_{p,i}$ (Yu et al., 2006). The average pore size relates to the particle surface area as $d_{p,i} = 1/S_i\rho_i$ where $S_p = S_c = 0.05$ m^2/g and $S_a = 0.2$ m^2/g (de Jonge and Mittelmeijer-Hazeleger, 1996). The absolute permeability of soil media can be estimated from the empirical expression (Punmia and Jain, 2005)

$$K_i = 10^{-3} d_{p,i}^2 \sim 1/\rho_i^2 \tag{14}$$

which varies from 10^{-12} to 10^{-9} m^2, and decreases with the bulk density.

Because of a high porosity of ($\psi_p = 0.867$), and the low volumetric water content, water is assumed to stay in the pores of peat without volume expansion. Thus, the wet peat bulk density is calculated as $\rho = (1 + \text{MC})\rho_p$. The properties of α-char and β-char are assumed to be the same.

The kinetic parameters of a low-mineral (IC $\approx$ 2%) moss peat sample from Ireland (Huang and Rein, 2016) is selected for a case study, listed in Table 2. Abundant experiment

2. The radiation across pores plays an important role in heat transfer of porous media, while the pure conduction becomes weak because of the discontinuity in the solid phase.

Table 2: Reaction parameters and yields of 5-step reactions for the Irish peat sample (Huang and Rein, 2016) where $\Delta H > 0$ (endothermic) and $\Delta H < 0$ (exothermic).

Parameter/k	dr	pp	po	βo	αo
lg A_k (lg(s^{-1}))	6.91	8.18	16.8	7.38	13.3
E_k (kJ/mol)	58.7	112	195	117	172
n_k (-)	2.37	5.31	2.33	1.32	2.58
n_{k,O_2} (-)	-	-	0.24	0.52	0.86
$\nu_{B,k}$ (kg/kg)	0	0.28	0.61	0.04	0.07
ΔH_k (MJ/kg)	2.26	0.5	-11.6	-28.9	-27.8
$\nu_{O_2,k}$ (kg/kg)	0	0	0.89	2.21	2.12

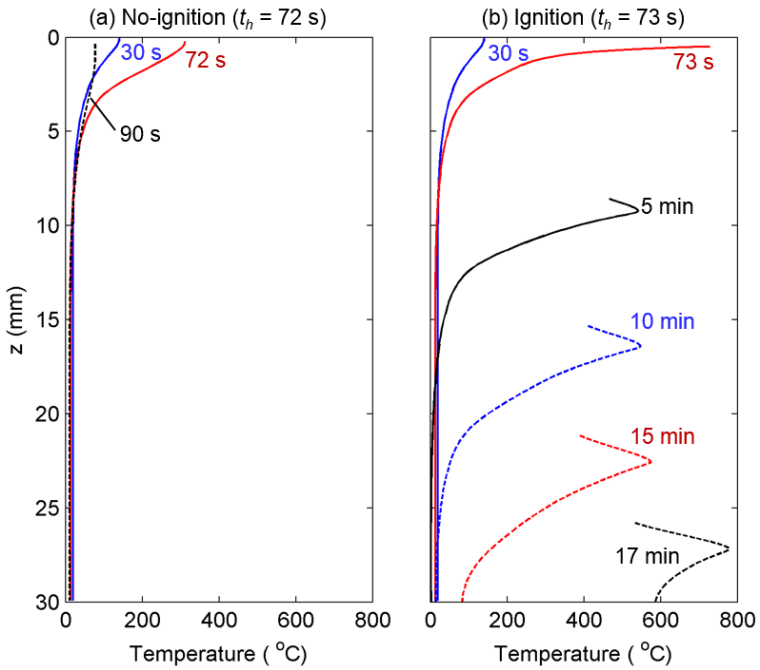

Figure 2: Evolution of the predicted temperature profile in the case of (a) no-ignition ($t_h = 72$ s), and (b) ignition ($t_h = 73$ s), where peat moisture content is MC = 80%, and oxygen concentration is $X_{O_2} = 28\%$.

data of this moss peat is available in the literature (Hadden et al., 2013; Belcher et al., 2010; Huang et al., 2016) to compare with and validate the modelling results. The heat of pyrolysis is $\Delta H_{pp} = 0.5$ MJ/kg (endothermic); the heat of oxidation is assumed to be proportional to its yield, $\Delta H_k = \Delta H_{O_2}(1 - \nu_{B,k}) < 0$ (exothermic). According to the DSC analysis of multiple peat samples in Bergner and Albano (1993), $\Delta H_{O_2} = -30$ MJ/kg is estimated for this low-mineral moss peat. The oxygen consumption is related to the heat of oxidation as $\nu_{O_2,k} = \Delta H_k/(\text{-}13.1$ MJ/kg) (Huggett, 1980).

3. Smouldering ignition

For the 3-cm peat sample (Fig. 1a), successful ignition is defined as the consumption of all organic matter. Figure 2 shows the predicted evolution of the temperature for an unsuccessful ignition, and a successful ignition, with the same MC = 80% and $X_{O_2} = 28\%$. For the no-ignition case (heating time $t_h = 72$ s), at the end of heating the peak temperature reaches 310 °C which is not high enough to form a smouldering front. After this, the temperature profile decreases to room temperature. For the ignition case (heating time $t_h = 73$ s), at the end of heating, the peak temperature exceeds 600°C, high enough to generate a smouldering front (Rein et al., 2008; Rein, 2013). Smouldering then consumes all the fuel within 20 min, showing a clear difference to the no-ignition case.

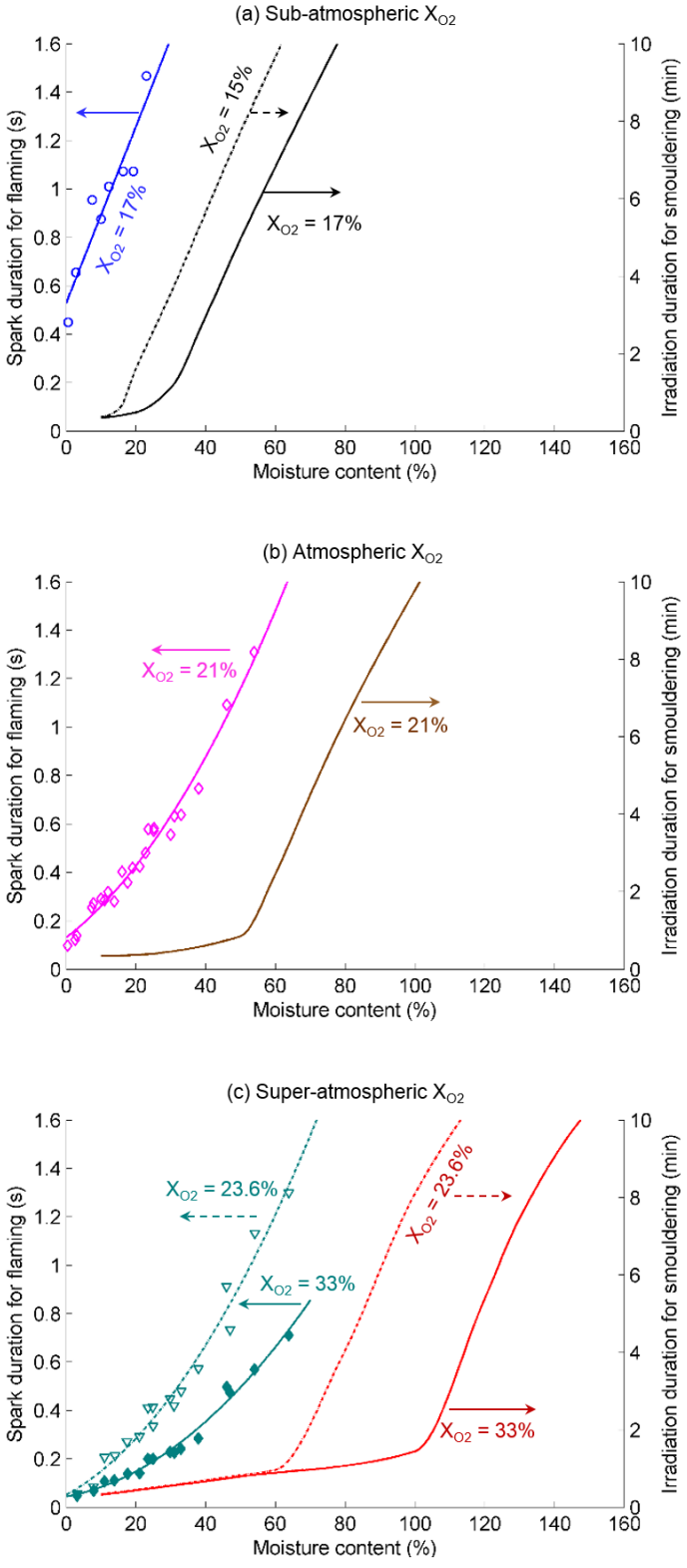

Figure 3: Comparison of critical ignition time vs. fuel moisture for flaming ignition of paper in experiments of Watson and Lovelock (2013) (points and fitting curve) and irradiation of peat smouldering by predictions (curve) at (a) sub-atmospheric $X_{O_2} < 21\%$; (b) atmospheric $X_{O_2} = 21\%$; and (c) super-atmospheric $X_{O_2} > 21\%$. Note that time scales are different for flaming and smouldering case.

Figure 3 shows the predicted heating duration vs. MC, compared with the flaming work of Watson and Lovelock (2013). As expected, in order to ignite a wetter fuel or at a lower-oxygen atmosphere, a longer heating duration is required for both flaming and smouldering. The comparison shows that under the same X_{O_2}, smouldering can be initiated in a fuel of MC $> 100\%$, substantially higher than flaming (MC $< 70\%$). More importantly, smouldering can be ignited in a low oxygen environment where flaming ignition is not possible. Dry paper was found not to hold a flame in $X_{O_2} < 17\%$, while peat with MC $= 30\%$ or 10% can still be ignited at $X_{O_2} = 15\%$ and 13%, respectively. These predictions agree with the experiments in Hadden et al. (2013), where dry peat (MC $\approx 10\%$) was ignited at $X_{O_2} = 13\%$. Therefore, compared to flaming fires, smouldering fires have a much lower X_{O_2} and MC thresholds.

It is also found that for both flaming and smouldering ignition, the required heating duration increases with MC faster than greater than linear. Modelling results show that as MC increases up to an elbow point, the required heating duration (t_h) increases significantly, and the MC^*_{ig} at the elbow point also increases with oxygen concentration. In this region of high MC^*, if the heating duration is slightly below the curve, a smouldering front can be formed and spread for a small distance, rather than experiencing extinction as Fig. 3(a). Such non-sustained smouldering spread is sensitive to the sample thickness and bottom boundary condition. Once the smouldering front is generated, the effect of the external heating is weak. This was also observed in the experiments of Hadden et al. (2013). Therefore, MC^* relates to extinction, noted as MC^*_{ex} (Huang and Rein, 2015). This is discussed and compared with MC^*_{ig} in the following section.

4. Spread and extinction of smouldering

For the 12-cm thick peat sample, a strong ignition protocol of 30 kW/m^2 for 3 min is applied to ensure the ignition of the top 1-cm dried peat layer (MC $= 10\%$). It can be seen that in Fig. 4, after 3 min of irradiation, the temperature profile 600 °C (similar to Fig. 2b), indicating that smouldering ignition is successful. Afterwards, if the atmospheric oxygen is too low or the 11-cm bottom layer is too wet, smouldering spread cannot be sustained, and the fire extinguishes after spreading for a short distance (Fig. 4a). This extinction is very different from the sudden cooling of the no-ignition cases (Fig. 2a). If ignited and not extinguished, smouldering spreads vertically across the wet peat up to the end of the sample (Fig. 4b). Therefore, the critical peat moisture (MC^*_{ex}) and critical oxygen concentration ($X^*_{O_2}$) for extinction are determined as the values for which just before the fire cannot consume the whole sample.

The vertical spread rate is not a constant, but monotonically decreases with depth. Therefore, for easy of comparison, the average spread rate between 3 and 6 cm deep is used as characteristic spread rates. Figure 5 shows the predicted characteristic spread rate for smouldering as a function of X_{O_2} and MC, where the interactions between oxygen concentration and MC is captured.

Figure 5 shows that smouldering spread increases in oxygen-richer atmospheres, while decreasing over wetter fuels, similar to the flaming spread in Watson and Lovelock (2013). At the same time, a critical curve ($X^*_{O_2}$ vs. MC^*) for smouldering spread is shown. Beyond the critical curve, fire spread cannot be sustained, and the spread rate quickly drops from about 0.5 mm/min to zero. Within the critical curve, the predicted spread rate of smouldering is

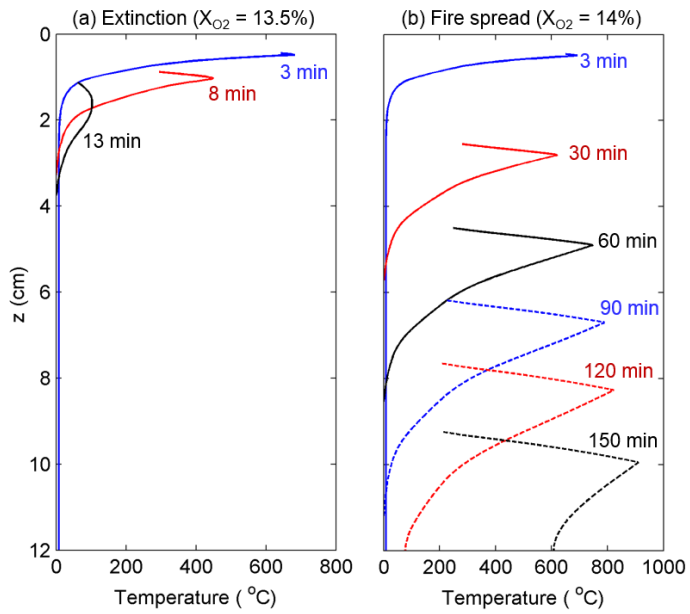

Figure 4: Evolution of the predicted temperature profile in the case of (a) extinction ($X_{O_2} = 13.5\%$), and (b) spread ($X_{O_2} = 14\%$), where the MC of the wet bottom peat is 40%.

on the order of 1 mm/min, similar to experimental measurements in Huang et al. (2016), while is at least 2 orders of magnitude slower than flaming fires in Watson and Lovelock (2013).

Figure 6 summarizes the predicted critical curves of MC* vs. $X^*_{O_2}$ for both smouldering ignition and spread. For smouldering ignition, a fixed ignition protocol (30 kW/m^2 for 90 s) is modelled. For comparison, Fig. 6 also includes the experiments of flaming paper (Watson and Lovelock, 2013) and smouldering peat (Belcher et al., 2010; Hadden et al., 2013). Clearly, for both flaming and smouldering, MC* increases with $X^*_{O_2}$, indicating that

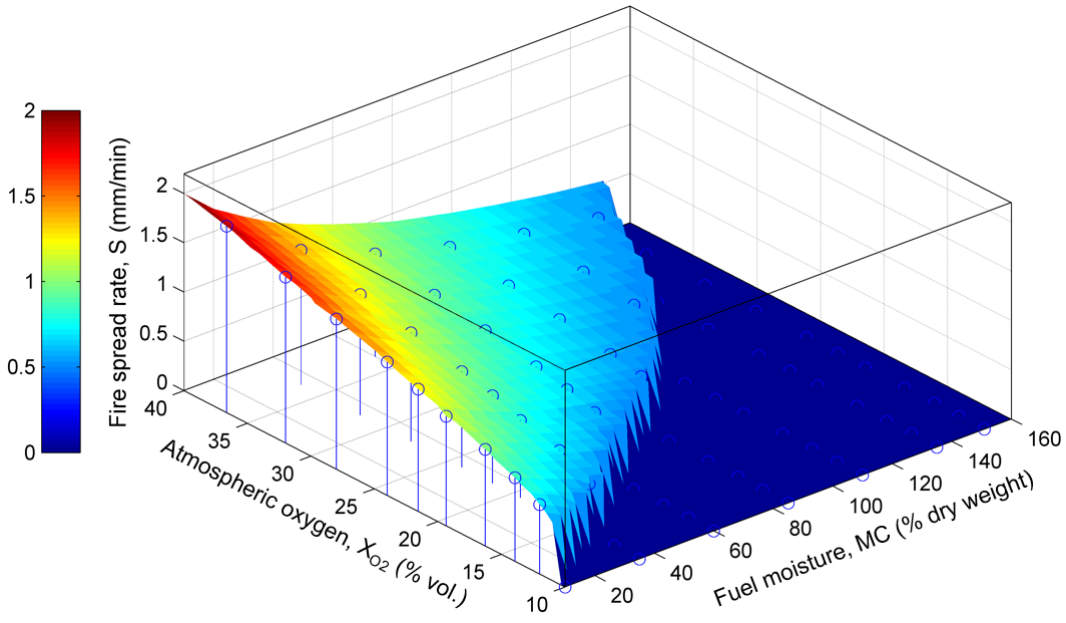

Figure 5: Smouldering spread rate as a function of atmospheric oxygen concentration (X_{O_2}) and fuel moisture content (MC). The color visualizes the rate of smouldering spread, which increases from blue to red.

fire risk increases significantly in an oxygen-enriched environment.

Each of the smouldering ignition experiments in Hadden et al. (2013) and smouldering spread experiments in Belcher et al. (2010) was with fixed peat MC (dry) which provides two points in Fig. 6. Note that these two experiments used the same peat, and physico-chemical parameters of this peat are the input to the model. It can been seen that both points are close to model predictions, suggesting a validation of the modelling results for low-MC and low-X_{O_2} ranges. It is also observed that for both flaming and smouldering, the MC^*_{ig} is lower than MC^*_{ex}, and their difference increases with MC and X_{O_2}. More discussions on MC^*_{ig} and MC^*_{ex} can be found in Huang and Rein (2015).

At both high MC and X_{O_2}, there is a nonlinear correlation. The required X_{O_2} increases faster than MC, which may be a result of the complex interaction among heat transfer, oxygen supply, and smouldering chemistry. These nonlinear fire thresholds are also observed in flaming experiments. Therefore, the linear correlation, $\mathrm{MC}^* = 8X^*_{O_2} - 128$, presented in Watson and Lovelock (2013) and included in Fig. 6, becomes inaccurate at high MC and X_{O_2}. Overall, it is revealed that compared to flaming spread, smouldering spread can be sustained in substantially lower X_{O_2} (as low as 12%), and in a substantially higher MC ($> 100\%$). Therefore, it is smouldering, rather than flaming, defines the lower threshold for Earth fire activity throughout geological times.

5. Conclusions

The dependence of smouldering fires in peatlands, the largest wildfires on Earth, with atmospheric oxygen is investigated using a physics-based computational model. Modelling

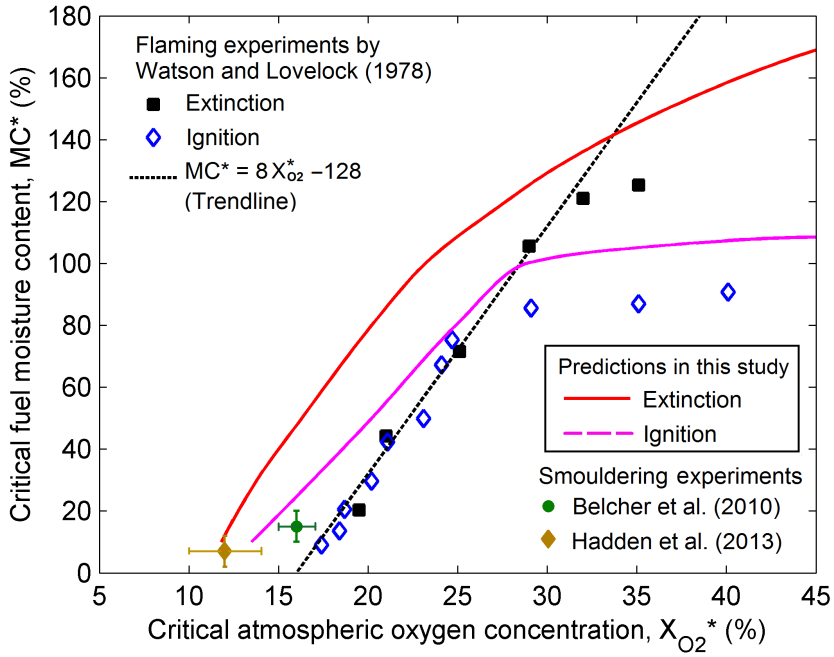

Figure 6: Critical moisture content (MC^*) vs. critical ambient oxygen concentration ($X^*_{O_2}$) found in experiments of flaming paper (Watson and Lovelock, 2013) and smouldering peat (Belcher et al., 2010; Hadden et al., 2013), and new predictions. In experiments, the uncertainty of peat MC comes from the bound water remained after drying and the potential absorption of atmospheric moisture, and the uncertainty in $X^*_{O_2}$ comes from various criteria to judge successful ignition or fire spread.

results reveal a novel nonlinear correlation between the critical oxygen concentration and moisture content. As moisture content increases, a greater increase in oxygen concentration is required for both ignition and fire spread. More importantly, compared to flaming fires in the literature, smouldering fires can be ignited in a substantially higher fuel moisture content (MC $>$ 100%), and at a substantially lower oxygen concentration ($X_{O_2} \sim 12\%$), defining a much lower wildfire threshold in Earth history.

For smouldering fires, we also found that the critical curve of MC* and $X^*_{O_2}$ for extinction is higher than that for ignition. The smouldering spread increases in oxygen-richer atmospheres, while decreasing over wetter fuels, in agreement with flaming fires. The predicted spread rate of smouldering peat fire is on the order of 1 mm/min, much slower than flaming fires. This is the first time a sophisticated physics-based model is used to study interactions among atmospheric oxygen, fuel moisture and smouldering wildfires, and to compare with flaming fires. Thus, it helps understand the char remains and historical fire activities seen in the fossil record.

Acknowledgements

The authors would like to thank Dr Claire Belcher (University of Exeter) and Dr Rory Hadden (University of Edinburgh) for useful discussions.

References

Belcher, C.M., McElwain, J.C.. Limits for Combustion in Low O_2 Redefine Paleoatmospheric Predictions for the Mesozoic. Science 2008;321(5893):1197–1200.

Belcher, C.M., Yearsley, J.M., Hadden, R.M., McElwain, J.C., Rein, G.. Baseline intrinsic flammability of Earths ecosystems estimated from paleoatmospheric oxygen over the past 350 million years. Proceedings of the National Academy of Sciences 2010;107(52):22448–22453.

Benscoter, B.W., Thompson, D.K., Waddington, J.M., Flannigan, M.D., Wotton, B.M., de Groot, W.J., Turetsky, M.R.. Interactive effects of vegetation, soil moisture and bulk density on depth of burning of thick organic soils. International Journal of Wildland Fire 2011;20:418–429.

Bergner, K., Albano, C.. Thermal analysis of peat. Analytical Chemistry 1993;65(3):204–208.

Frandsen, W.H.. Ignition probability of organic soils. Canadian Journal of Forest Research 1997;27(9):1471–1477.

Hadden, R.M., Rein, G., Belcher, C.M.. Study of the competing chemical reactions in the initiation and spread of smouldering combustion in peat. Proceedings of the Combustion Institute 2013;34(2):2547 – 2553.

Huang, X., Rein, G.. Smouldering combustion of peat in wildfires: Inverse modelling of the drying and the thermal and oxidative decomposition kinetics. Combustion and Flame 2014;161(6):1633 – 1644.

Huang, X., Rein, G.. Computational study of critical moisture and depth of burn in peat fires. International Journal of Wildland Fire 2015;24:798 – 808.

Huang, X., Rein, G.. Thermochemical conversion of biomass in smouldering combustion across scales: The roles of heterogeneous kinetics, oxygen and transport phenomena. Bioresource Technology 2016;207:409 – 421.

Huang, X., Rein, G., Chen, H.. Computational smoldering combustion: Predicting the roles of moisture and inert contents in peat wildfires. Proceedings of the Combustion Institute 2015;35(3):2673 – 2681.

Huang, X., Restuccia, F., Gramola, M., Rein, G.. Experimental Study of the Formation and Collapse of an Overhang in the Surface Spread of Smouldering Peat Fires. Combustion and flame 2016;(in press).

Huggett, C.. Estimation of rate of heat release by means of oxygen consumption measurements. Fire and Materials 1980;4(2):61–65.

Jacobsen, R., Lemmon, E., Penoncello, S., Shan, Z., Wright, N.. Thermophysical Properties of Fluids and Materials. In: Bejan, A., Kraus, A., editors. Heat Transfer Handbook. John Wiley & Sons; 2003. p. 43–159.

de Jonge, H., Mittelmeijer-Hazeleger, M.C.. Adsorption of CO_2 and N_2 on Soil Organic Matter: Nature of Porosity, Surface Area, and Diffusion Mechanisms. Environmental Science & Technology 1996;30(2):408–413.

Lautenberger, C., Fernandez-Pello, C.. Generalized pyrolysis model for combustible solids. Fire Safety Journal 2009;44(6):819 – 839.

Lenton, T.M.. Fire Feedbacks on Atmospheric Oxygen. In: Belcher, C., editor. Fire Phenomena and the Earth System. John Wiley & Sons; 2013. p. 289–308.

Lenton, T.M., Watson, A.J.. Redfield revisited: 2. What regulates the oxygen content of the atmosphere? Global Biogeochemical Cycles 2000;14(1):249–268.

Lovelock, J.. Gaia, a new look at life on earth. Oxford paperbacks. Oxford University Press, 1979.

Lovelock, J.E., Lodge, J.P.. Oxygen in the contemporary atmosphere. Atmospheric Environment 1972;6(8):575 – 578.

Ohlemiller, T.. Modeling of smoldering combustion propagation. Progress in Energy and Combustion Science 1985;11(4):277 – 310.

Punmia, B., Jain, A.. Soil Mechanics and Foundations. Laxmi Publications Pvt Limited, 2005.

Rein, G.. Smouldering Fires and Natural Fuels. In: Belcher, C., editor. Fire Phenomena and the Earth System. Wiley and Sons; 2013. p. 15–33.

Rein, G., Cleaver, N., Ashton, C., Pironi, P., Torero, J.L.. The severity of smouldering peat fires and damage to the forest soil. Catena 2008;74(3):304 – 309.

Watson, A.J., Lovelock, J.E.. The Dependence of Flame Spread and Probability of Ignition on Atmospheric Oxygen. In: Belcher, C., editor. Fire Phenomena and the Earth System. John Wiley & Sons; 2013. p. 273–287.

Watts, A.C.. Organic soil combustion in cypress swamps: Moisture effects and landscape implications for carbon release. Forest Ecology and Management 2013;294:178 – 187. The Mega-fire reality.

Wildman, R.A., Hickey, L.J., Dickinson, M.B., Berner, R.A., Robinson, J.M., Dietrich, M., Essenhigh, R.H., Wildman, C.B.. Burning of forest materials under late Paleozoic high atmospheric oxygen levels. Geology 2004;32(5):457–460.

Yu, F., Wei, G., Zhang, X., Chen, K.. Two Effective Thermal Conductivity Models for Porous Media with Hollow Spherical Agglomerates. International Journal of Thermophysics 2006;27(1):293–303.

Nomenclature

c	heat capacity
d_p	characteristic pore size
E	activation energy
h	enthalpy
h_c	convective coefficient
h_m	mass-transfer coefficient
ΔH	heat of reaction
k	thermal conductivity
K	permeability
L	sample size
$\dot{m}''$	mass flux
n	reaction order
P	pressure
$\dot{q}''$	heat flux
R	gas constant
S	particle surface area
t	time
T	temperature
X_{O_2}	oxygen concentration, percentage by volume (%)
X	volume fraction
Y	mass fraction
z	distance
Z	pre-exponential factor

Greeks

γ	radiative coefficient
δ	thickness
ε	emissivity
κ	radiation absorption coefficient
ν	stoichiometric coefficient
ρ	density
σ	Stefan-Boltzmann const.
χ	fraction factor
ψ	porosity
$\dot{\omega}$	reaction rate

Superscripts

$*$	critical or normalized

Subscripts

0	initial
α	α-char
β	β-char
a	ash
d	destruction
dr	drying
f	formation
ex	extinction
g	gas
i	condensed species number
ig	ignition
j	gaseous species number
k	reaction number
o	oxidation
p	peat or pyrolysis
s	solid or source
sm	smouldering
w	water